Mathematical Biosciences and Engineering

MBE, 19(6): 6186–6203.
DOI: 10.3934/mbe.2022289
Received: 20 February 2022
Revised: 24 March 2022
Accepted: 25 March 2022
Published: 15 April 2022

http://www.aimspress.com/journal/MBE

Research article

Study on seafloor hydrothermal systems circulation flow and heat transfer characteristics

Yi Ren[1], Guolei Zhang[1,*], Longbin Yang[1,*], Yanwei Hu[2], Xiaojing Nie[1], Zhibin Jiang[1], Dawei Wang[1] and Zhifan Wu[1]

[1] College of Power and Energy Engineering, Harbin Engineering University, Harbin, MO 150001, China
[2] School of Energy Science and Engineering, Harbin Institute of Technology, Harbin, MO 150001, China

* **Correspondence:** Email: zhangguolei@hrbeu.edu.cn, yanglb@hrbeu.edu.cn; Tel: +8613766860906, +8613936138853.

Abstract: In this work, the numerical simulation study of the hydrothermal flow and heat transfer process in the porous rock under 30 MPa pressure was developed. The flow and heat transfer characteristics of hydrothermal in rocks with different porosities are studied by changing the porosity of the rock. The simulation results show that the average flow velocity decreases and the average temperature increases when the porosity decreases. The velocity field and temperature field are coupled due to the nonlinear thermophysical properties of hydrothermal. The velocity field and temperature field have strongly interacted in the range of 400–450 ℃ and the effect of temperature on velocity is gradually diminishing outside the range. Most of the fluid will be "squeezed" into the crevice and the average velocity is almost three times the no-creviced case when a crevice is present. The existence of the crevice makes the total heat flux decrease from an overall perspective, and the crevice makes a large temperature gradient at the entrance and export of the crevice from a local perspective. These results provide theoretical support for the utilization of submarine hydrothermal fluid shallow circulation heat energy.

Keywords: hydrothermal convection; porous rock; numerical simulation

1. Introduction

Elder [1] found that there are two different heat transfer mechanisms in the ocean and he divided

the ocean into two major regions: "normal areas" and "thermal areas", then he proposed the hydrothermal system in the "thermal areas" for the first time in 1965. Corliss et al. [2] took the "Alvin" deep submersible to observe the hydrothermal activity of the seabed in the Galapagos Rift, this discovery immediately aroused the interest of scientists in the study of the distribution characteristics, formation causes, environmental effects, and the mechanism of mineral activity in the submarine hydrothermal area. As the hydrothermal activities research work went further and more detailed, scientists found hydrothermal fluids have high application value and development potential in many fields. For example, Schultz et al. [3] find temperature change of the hydrothermal vent has a certain synchronization with geological activities such as submarine earthquakes. Carol et al. [4] pointed out that the total global ocean heat flux can be 3.2×10^{13} W of which nearly 34% is contributed by the hydrothermal cycle, which means the amount of heat released by the hydrothermal fluid is comparable to that released by volcanic eruption [5]. The submarine hydrothermal fluid contains a huge amount of heat energy, and it will provide innovation for solving the human energy crisis if this part of the energy can be collected and utilized.

The formation mechanism of seafloor hydrothermal fluid is: Seawater enters the crevice at the seafloor and is heated up by rocks while it flows down. Fluid density decreases when the temperature increases, then seawater returns to the seafloor as hydrothermal fluid. The process of cold seawater being heated by porous rocks is the power and heat source of the entire submarine hydrothermal cycle, therefore, there has been a flurry of investigations on this process. Peter [6] proposed a spatiotemporal continuous transport model for hydrothermal, and he obtained the analytical expressions for porosity and permeability with time under quasi-steady-state conditions. Davis et al. [7] analyzed three cruise surveys dates which obtain from the Cascadia Basin, he found that cementation will change the rock permeability which was caused by hydrothermal mineral precipitation. Bessler et al. [8] conducted a numerical simulation on hydrothermal convection in a sedimentary ridge environment and discussed the convection of hydrothermal fluid in different rock permeability. Taylor et al. [9] used the numerical simulation method to study the hydrothermal fluid flows in porous media. Jupp and Schultz [10] used the numerical simulation method to explain the reason why the vent temperature (350–400 ℃) of "black smokers" is lower than the magma temperature (1200 ℃). Davis [11] used a two-dimensional finite element convection model to calculate the fluid velocity distribution of the hydrothermal cycle and the results showed that there is a long horizontal flow section in the shallow hydrothermal cycle. The results of Fontaine et al. [12] confirmed the second conclusion obtained by Davis: the porous rock in the shallow hydrothermal fluid circulation has a higher permeability which leads to a uniform horizontal temperature distribution of the porous rock. Crone et al. [13] applied the one-dimensional model of tidal loads on the poroelastic medium half-space in Jupp [14] to study the influence of ocean tidal loads on the shallow hydrothermal fluid circulation system. Wilcock [15] uses a porous convection model to study the circulation pattern and the relationship between permeability and temperature, his results show the bottom temperature ratio is between 0.5 and 0.65 but the ratio will be reduced for porous rocks with high permeability.

Jiang et al. [16] summarized the research status of the seepage characteristics of rock crevices domestic and abroad in his paper, and he said: "No standard equations have been formed to study the coupling characteristics of seepage and stress in rock crevices". Jiang's analysis provides a direction for future research on the seepage characteristics of rock crevices. Ma et al. [17] obtained the permeability of rock samples with different crevices and pore combinations under steady flow and unsteady flow conditions. The seepage channels of the rock increase with the increase of the rock size

after Ma analyzed the permeability characteristics of multi-scale rocks, which will result in the permeability increases. This permeability law is important and instructive for practical engineering. Zhang et al. [18] elaborated on the research progress of the heat transfer at supercritical pressure in porous media from experimental research and numerical simulation, respectively. He pointed out that the influence of property changes and tortuous flow channels on heat transfer is a direction of future research.

Table 1. List of symbols.

Symbol	Property	Units
T	Temperature	°C
P	Pressure	Pa
γ	Porosity of rock	—
V_P	Volume of pores	m^3
V_B	Total volume of rock	m^3
α	Permeability of rock	m^2
ρ	Density	$kg·m^{-3}$
ρ_f	Liquid density	$kg·m^{-3}$
ρ_s	Rock density	$kg·m^{-3}$
$\vec{u}$	Darcy velocity	$m·s^{-1}$
u	velocity at y = 0.5 cm line	$m·s^{-1}$
$\overline{\tau}$	Stress tensor	Pa
$\vec{g}$	Gravitational acceleration	$m·s^{-2}$
μ	molecular viscosity	Pa·s
C_2	Inertial resistance factor	m^{-1}
E_f	Total fluid energy	$kJ·kg^{-1}$
E_s	Total solid medium energy	$kJ·kg^{-1}$
u_m	Average cross-sectional velocity	$m·s^{-1}$
C_p	Specific heat capacity at constant pressure	$kJ·(kg·K)^{-1}$
θ	Excess temperature	—
q_w	Heat flux from wall	$kJ·(s·m^2)^{-1}$
T_w	Wall temperature	°C
$T_{y=0.5}$	The temperature at y = 0.5 cm line	°C
T_m	Average cross-sectional temperature	°C
Nu_x	Local Nusselt number	—
h_x	Local convective heat transfer coefficient	$W·(m^2·°C)^{-1}$
l	Characteristic length	m

Epping et al. [19] stated "At present, most of the numerical studies have focused on the physical or chemical aspects of hydrothermal activity, while greatly simplifying the thermodynamic effects on shallow hydrothermal circulation". The permeability of ocean crust plays a key role in hydrothermal

circulation [20], and porous media can enhance the heat transfer rate to a certain extent [21]. Therefore, the research content of this paper is the flow and heat transfer characteristics of shallow hydrothermal circulation in porous rocks at a depth of 3000 m. Numerical simulation methods are used to study the flow and heat transfer characteristics of hydrothermal in porous rocks. This research can provide theoretical support for the utilization of submarine hydrothermal fluid shallow circulation heat energy.

2. Establishment of numerical and physical models

2.1. Numerical model

Main parameters of porous rock:

1) Porosity. Porosity represents the ratio of the pore volume in the porous rock to the total volume of the rock, the equation is:

$$\gamma = \frac{V_P}{V_B} \times 100\% \tag{1}$$

V_P represents the volume of pores, and V_B represents the total volume of porous rock.

2) Permeability. The permeability of porous rock determines the value of the viscous resistance coefficient of fluid flow in porous media. Permeability is a physical quantity that can directly represent the ease of flow, especially for low-speed flow. However, it is difficult to obtain permeability directly through measurement methods. In engineering, the corresponding empirical formula of permeability is generally given by fitting a large amount of experimental data. This paper uses the sampling data of Zhang et al. [22] and Niu et al. [23] to estimate rock permeability. The result is shown in Table 2.

Table 2. Main parameters of porous rock in different conditions.

Conditions	Porosity	Permeability
Case 1	γ=0.2	$\alpha = 3.737\times10^{-10}\ m^2$
Case 2	γ=0.15	$\alpha = 4.878\times10^{-11}\ m^2$
Case 3	γ=0.1	$\alpha = 6.636\times10^{-12}\ m^2$

2.2. Control equation

Since the pore size of the investigated rock is more than 100 μm, which belongs to the macro-scale [24], the following equations are chosen as the governing equation of the fluid.

Continuity equation:

$$\frac{\partial}{\partial t}(\gamma\rho_f) + \nabla(\gamma\rho_f\vec{u}) = 0 \tag{2}$$

Momentum equation:

$$\frac{\partial}{\partial t}(\gamma\rho_f\vec{u}) + \nabla(\gamma\rho_f\vec{u}\vec{u}) = -\gamma\nabla p + \nabla(\gamma\overline{\tau}) + \gamma\rho_f\vec{g} - (\frac{\gamma^2\mu}{\alpha}\vec{u} + \gamma^3 C_2\frac{1}{2}\rho_f|u|\vec{u}) \quad (3)$$

Energy equation:

$$\frac{\partial}{\partial t}(\gamma\rho_f E_f + (1-\gamma)\rho_s E_s) + \nabla(\vec{u}(\rho_f E_f + p)) = \nabla[\lambda_{eff}\nabla T + (\overline{\tau}\vec{u})] \quad (4)$$

2.3. Physical model

The model of the non-creviced porous rock is shown in Figure 1. The geometric size is 20 cm × 1 cm. The initial conditions and boundary conditions of the calculation domain are as follows: In the entire calculation domain, the entire flow field is in a static state at the initial moment and the operating pressure is 30 MPa, the operating temperature is 4 ℃, the inlet type is pressure inlet, the inlet pressure is 300 Pa, the inlet temperature is 400 ℃, and the wall temperature is taken as the constant, the value is 550 ℃ (according to the research results of Saccocia et al. [25]), the outlet as pressure outlet and the outlet pressure is 0 Pa, the outlet temperature is set to 550 ℃.

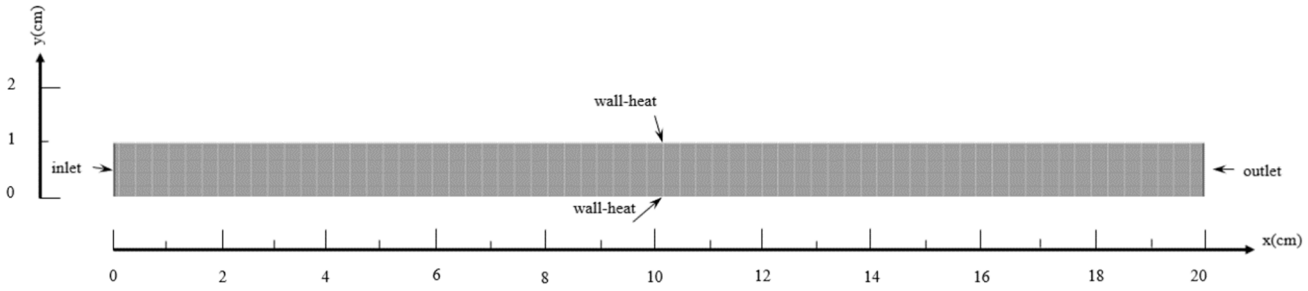

Figure 1. Schematic diagram of non-crevice porous rock grid.

Hydrothermal circulation mostly exists in areas where geological activities are very active, these geological activities will cause the formation of crevices in the porous rock. The appearance of crevices will inevitably affect the flow and heat transfer characteristics of the hydrothermal fluid in the porous rock. Therefore, it is necessary to simulate the existence of the crevice in porous rocks.

The calculation model of the creviced porous rock is shown in Figure 2. The geometric size is 20 cm × 1 cm, and the crevice size is 0.2 cm × 7 cm. The initial conditions and boundary conditions of the calculation domain are the same as the non-creviced porous rock.

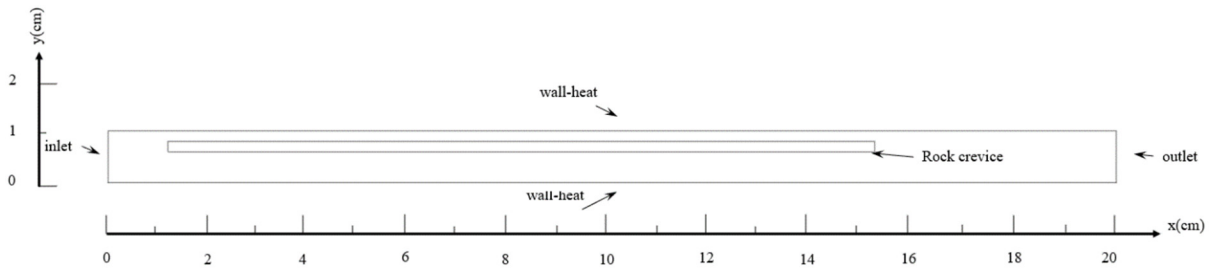

Figure 2. Schematic diagram of porous rock with a single crevice model.

2.4. Numerical solution settings

1) Assuming that the matrix part is isotropic;
2) Assuming that the hydrothermal fluid is incompressible;
3) Ignore the viscous dissipation, thermal dispersion effects, and reversible work generated by fluid deformation in porous media;
4) Assuming that the fluid part and the solid skeleton in the porous rock are in a local thermal equilibrium state.

The fluid properties change drastically in the calculation domain because the temperature at the inlet and outlet changes greatly. Therefore, this article uses the NIST physical property function of the REFPROP software in FLUENT to define the physical properties of the hydrothermal fluid at different temperatures. The steady-state calculation is used for numerical simulation, uses the Semi-Implicit Method for Pressure Linked Equations (SIMPLE), and the pressure discretization scheme uses PRESTO! method. Since the grid used in this paper is a quadrilateral grid, the momentum equation, and energy equation both use the second-order upwind style. The residual of the continuity equation is controlled below $1e^{-8}$, and the residual of the energy equation is controlled below $1e^{-10}$. At the same time, the flow rate changes of the inlet and outlet are detected. It is considered that the calculation can be stopped when the inlet and outlet flow are stable and the residual meets the convergence conditions.

3. Results and discussion

3.1. Influence of porosity on flow and heat transfer characteristics

Rock porosity is related to a series of factors such as depth, geological activity, hydrothermal fluid physical properties, etc. Porosity is concentrated in the range of 0.05–0.2 in a depth of 3000 m according to Niu et al. [23]. The porosity will directly affect the permeability, the flow characteristics and heat transfer characteristics of the hydrothermal fluid. Therefore, this paper simulates rocks with different porosities to analyze the influence of porosity on the flow and heat transfer characteristics.

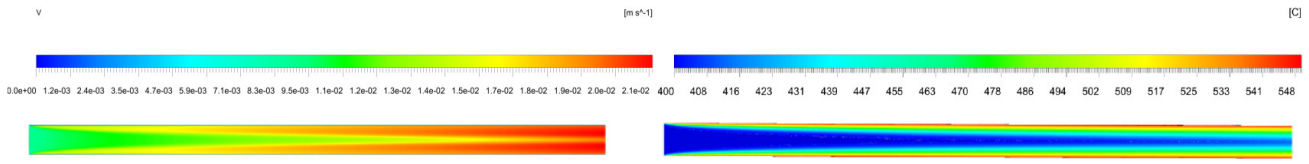

(a) case 1($\gamma = 0.20$, $\alpha = 3.737 \times 10^{-10}\ m^2$) velocity contours(left) and temperature contours (right)

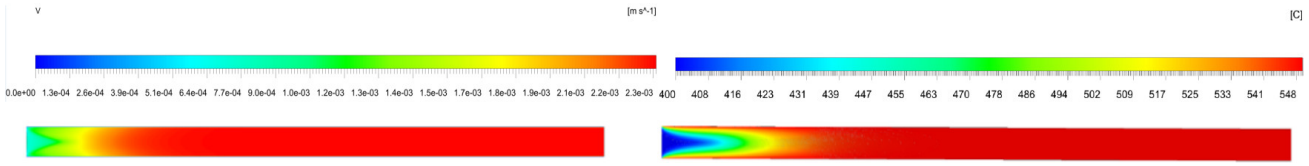

(b) case 2($\gamma = 0.15$, $\alpha = 4.878 \times 10^{-11}\ m^2$)velocity contours(left) and temperature contours (right)

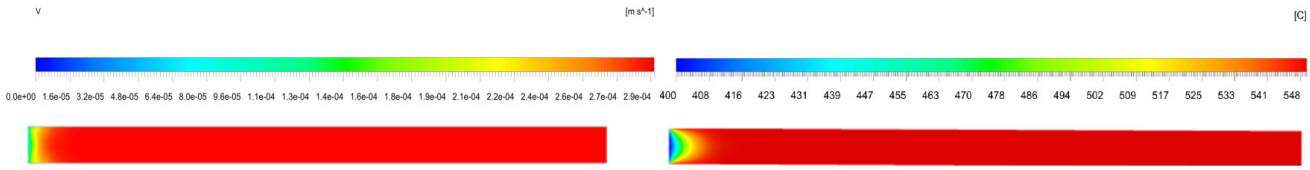

(c) case 3($\gamma = 0.10$, $\alpha = 6.636 \times 10^{-12}\ m^2$)velocity contours(left) and temperature contours (right)

Figure 3. Velocity and temperature contours of hydrothermal in the porous rock under different porosity without crevice.

Figure 3(a) shows the velocity and temperature distribution feature are both "low in the middle and high on both sides", and the velocity gradually increases along the *x*-direction in case 1. The average cross-section velocity at the inlet is 8.49 × 10^{-3} m/s, and the average cross-section velocity at the outlet is 2.03 × 10^{-2} m/s which is 2.4 times the inlet. The velocity at the centerline (y = 0.5 cm) increases from 9.0 × 10^{-3} m/s to 1.92 × 10^{-2} m/s in case1. The average cross-section temperature increased from 400.00 ℃ to 468.28 ℃ and the temperature at the centerline (y = 0.5 cm) increased from 400 °C to 413.02 °C in case1. The distribution feature of the velocity field and the temperature field are similar because the velocity field and temperature field are coupled. The velocity is affected by density and the density is related to temperature, so velocity is related to temperature due to the nonlinear thermophysical properties of hydrothermal in the temperature range of 400–550 ℃. Density increases with the decrease of temperature and decreases with the increase of temperature, so the velocity increases when temperature increases which results in the velocity field distribution will be so close to the temperature field.

Figure 3(b),(c) show that the average velocity decreases when the porosity decreases, and the velocity distribution feature is still low in the middle and high on both sides before the fluid reaches the isothermal flow state. It is found that the velocity and temperature field in case 2 and case 3 no longer have such an obvious correspondence after comparing the velocity contours and temperature contours. The impact of temperature on the fluid velocity is minimal because the density changes gently in the temperature range of 500–550 ℃. Therefore, the flow characteristics in case 2 and case 3 will be different from case 1.

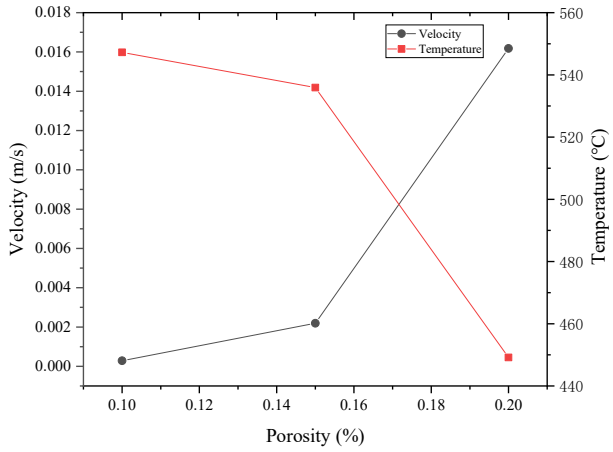

Figure 4. Variation of average velocity and average temperature under different porosity.

Figure 4 shows the average velocity is 2.19×10^{-3} m/s and 2.854×10^{-4} m/s in case 2 and case 3, respectively, and the average temperature is 535.917 and 549.253 °C, respectively. The flow time inside of the porous rock increases which makes the heat exchange between the hydrothermal and the porous rock more sufficient, so, the temperature distribution becomes uniform.

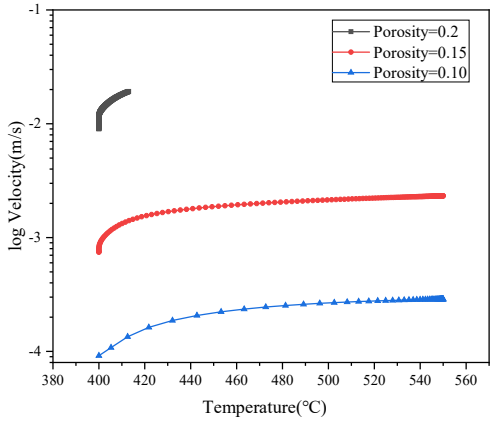

(a) Velocity at y = 0.5 cm as a function of temperature, velocity is given on the logarithmic scale.

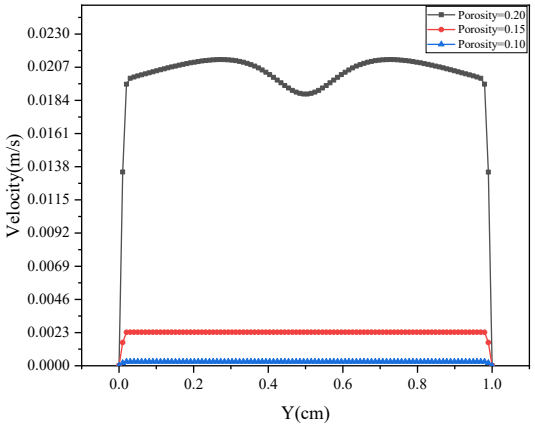

(b) Velocity at the outlet along the y-direction

Figure 5. Variation curve of velocity with temperature and y-direction under different porosity.

It can be seen from the above analysis that the velocity is not only related to the porosity but also corresponds to the nonlinear thermophysical properties of the hydrothermal fluid. Three laws can be seen in Figure 5. Firstly, the velocity increases with the increase of temperature in three cases from Figure 5(a), and the ratio of the maximum velocity to the minimum velocity is 3.1 in case 2 and case 3 which means the velocity increase rate is constant in case 2 and case 3. Secondly, the velocity gradient is the largest in the range of 400–450 °C, which indicates that the temperature field has the greatest impact on the velocity field in this range. Thirdly, Figure 5(b) shows the outlet velocity increase then decrease along the *y*-direction in case 1 but has been stabled in cases 2 and 3. The effect of temperature on the velocity is great at the outlet in case1because the flow hasn't reached the isothermal flow state. The temperature is evenly distributed along the cross-section before reaching the outlet in cases 2 and 3, and the temperature gradient on the entire cross-section at the outlet is 0, so the velocity is almost evenly distributed along the cross-section.

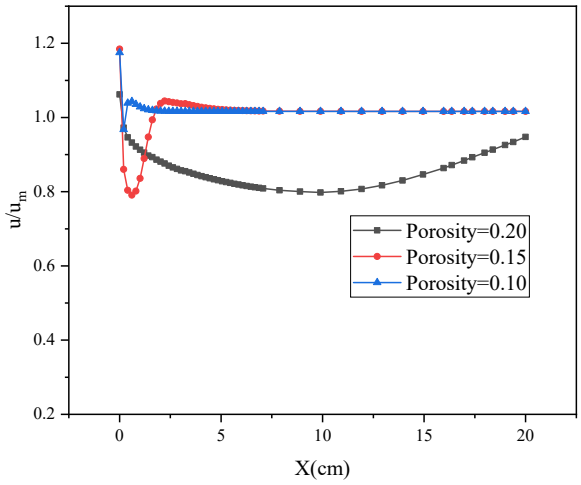

Figure 6. The dimensionless velocity curve at the location of $y = 0.5$ cm.

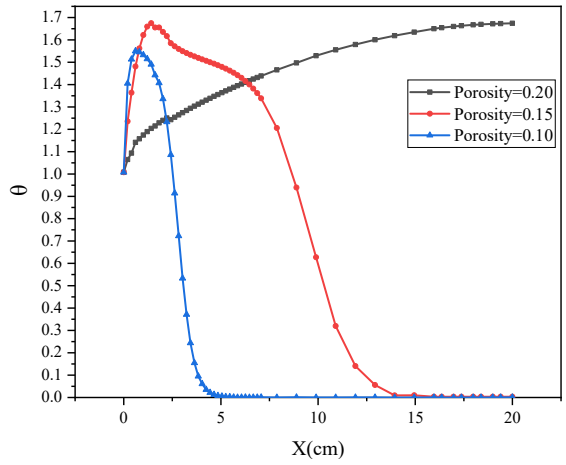

Figure 7. Excess temperature curve at the location of $y = 0.5$ cm.

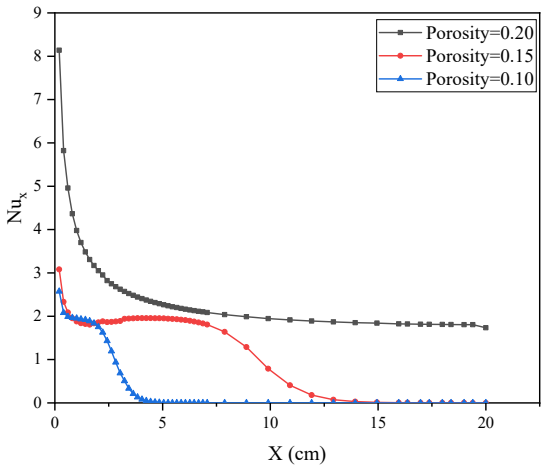

Figure 8. Local Nusselt number curve under different porosity.

Figure 6 is the dimensionless velocity at the y = 0.5 cm line (u_m is the average cross-sectional velocity), and the dimensionless velocity curve shows some different features from the constant property flow. The trends of the dimensionless velocity in cases 2 and 3 are both decreasing first and then increasing, finally decreasing. However, the trend of dimensionless velocity in case 1 is decreasing first and then increasing. The main factor affecting the hydrothermal velocity in the first decreasing section is temperature. The growth rate of u_m is larger than the growth rate of u because the temperature at the y = 0.5 cm line is the lowest along the y-direction, so the influence of temperature on u_m is larger than u. An interesting thing is that the average temperature corresponding to the end of the first decreasing section of these curves is 455.27 ℃ in case 1, 457.96 ℃ in case 2, and 460.75 ℃ in case 3, respectively, all of them have exceeded 450 ℃. In another word, the effect of temperature on velocity becomes less significant after these positions.

The factors affecting the hydrothermal velocity in the increasing section are the viscous resistance ($\mu\vec{u}/\alpha$) and fluid temperature at the y = 0.5 cm line. The average cross-section temperature has exceeded 450 ℃ when the increasing section appears, which means the u_m is less affected by temperature. At the same time, the fluid temperature is 432.37 ℃ at the position with coordinates (0.2,0.5) in case 3, 401.875 ℃ at the position with coordinates (0.8,0.5) in case 2, and 400.785 ℃ at the position with coordinates (9.9,0.5) in case1, respectively, which means the fluid velocity is still mainly affected by the temperature at these positions. Observing the curve in Figure 6, the dimensionless velocity at the beginning of the increasing section is less than 1which means u is lower than the u_m. On the other hand, the viscous resistance is a directly proportional effect on velocity, therefore, u increases fast under the action of temperature, and u_m increases slower than u because of the bigger viscous resistance. The second decreasing section only appeared in cases 2 and 3, and the main factor affecting velocity in this section is the viscous resistance. At the beginning of the second decreasing section, the fluid temperature is 453.072 °C at the position with coordinates (2.22,0.5) in case 2 and 473.255 °C at the position with coordinates (4.04,0.5) in case 3, respectively, which indicates that the temperature has a little impact on the flow velocity. The main reason affecting flow velocity is the viscous resistance in the second decreasing section. It can be seen from the curve in Figure 6 that the dimensionless velocity at the beginning of the second decreasing section has exceeded 1. Because under the action of viscous resistance, u will gradually approach u_m until two velocities are the same. There is no second decreasing section for case 1 because the two influencing factors of the

increasing section are still working on u and u_m.

Figure 7 is the excess temperature curve at the location of y = 0.5 cm ($\theta = \frac{(T_w - T_{y=0.5})}{(T_w - T_m)}$). The temperature at the y = 0.5 cm line rises more slowly than T_m because the temperature at the y = 0.5 cm line changes behind T_m. The excess temperature curve just shows an increasing section in case 1. This is because the temperature of the fluid has not fully developed, it will show the complete curve as in cases 2 and 3 if the flow distance is long enough.

Figure 8 shows the variation of the local Nusselt number curves for three cases. The definition of Nu_x is given as:

$$h_x = \frac{q_w}{T_w - T_m} = \frac{-\lambda_{eff} \frac{\partial T}{\partial y}\Big|_{y=0}}{T_w - T_m} \tag{5}$$

$$\frac{\partial T}{\partial y} = \frac{\partial (T - T_w)}{\partial y} = \frac{\partial \theta}{\partial y}(T_m - T_w) \tag{6}$$

$$h_x = \lambda_{eff} \frac{\partial \theta}{\partial y}\Big|_{y=0} \tag{7}$$

$$Nu_x = \frac{h_x l}{\lambda_{eff}} = l \frac{\partial \theta}{\partial y}\Big|_{y=0} \tag{8}$$

According to Figure 7, θ must be a function of x, and according to the definition of θ, θ is also a function of y, So θ is the function of x and y which can be written as $\theta(x, y)$. According to Eq (8), Nu_x is a function of x. Assuming $\theta(x, y)$ satisfies the S-L theorem, θ can be expressed as $\theta(x, y) = \theta_1(x)\theta_2(y)$. That means the Nu_x curve can reflect the trend of the $\theta_1(x)$ curve. Specifically, the trends with Nu_x and $\theta_1(x)$ should be the same. Figure 7 is the θ curve at y = 0.5 cm, that is $\theta(x, 0.5)$. So the trends of curves in Figures 7 and 8 should be the same. The "red" curve satisfies the same trend in the range of $4.24 \leq x \leq 20$ and the "blue" curve has the same trend in the range of $1.01 \leq x \leq 20$ in Figures 7 and 8, respectively. But the "black" curve has the opposite trend in the range of $0 \leq x \leq 20$ in Figures 7 and 8, respectively. After analyzing the simulation dates, the temperature of the "red" curve is 529.78 ℃ at the position with coordinates (4.24,0.5) and the average cross-sectional temperature is 536.68 ℃. The temperature of the "blue" curve is 533.35 ℃ at the position with coordinates (1.01,0.5) and the average cross-sectional temperature is 539.13 ℃. The average cross-sectional temperature of the "black" curve at x = 20 is 468.28 ℃. That means for the "red" and "blue" curves, the flow characteristics are similar to the constant physical properties of incompressible pipe flow after the position with coordinates (4.24,0.5) and (1.01,0.5), respectively. As for the "black" curve, the velocity field and the temperature field are still strongly interacted, which means the properties change drastically with temperature. Therefore, the "black" curve has the opposite trend in the range of $0 \leq x \leq 20$ in Figures 7 and 8, respectively.

3.2. The effect of the crevice on flow and heat transfer characteristics of hydrothermal

Figure 9 is a contour of pressure (notice the pressure is the relative pressure, the environment pressure is 30 MPa) distribution without crevice and with a single crevice in the porous rock, respectively. Figure 9 shows the pressure decreases uniformly when there is no crevice in the rock. Pressure is nearly a constant value from the beginning to the end of the crevice in the case of a single crevice, because the viscous resistance leads most of the fluid in the entire flow channel to be "squeezed" into the crevice to flow. (According to the simulation result, the flow velocity of the fluid in the crevice is 10^3 times that of the surrounding area)

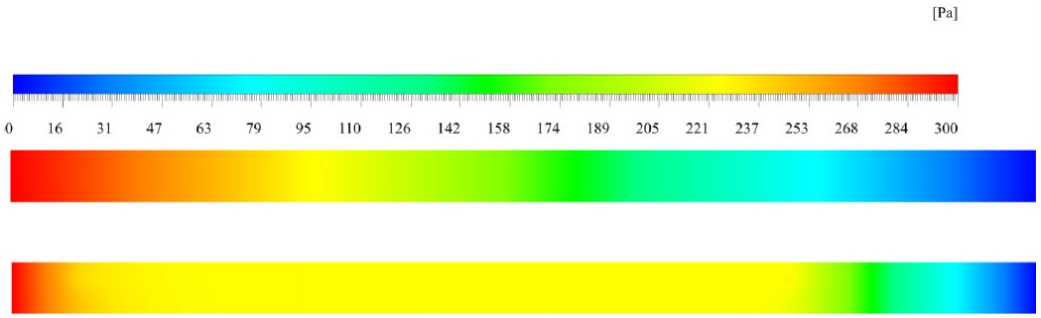

Figure 9. Pressure contours (case 1) without crevice (top) and with a single crevice (bottom), respectively.

Figure 10 is the velocity contours diagram and vector diagram of the entrance zone in cases without crevice and with a single crevice, respectively. It can be seen from (a) in Figure 10 that the velocity distributions of these cases are quite different. The flow velocity gradually increases with the increase of temperature, and the velocity distribution feature is low in the middle and high on both sides in the case of no crevice. The velocity is the highest among the crevice and it is evenly distributed across the entire section after the crevice disappears in the single crevice case. The average flow velocity of the two cases is 0.01615 m/s and 0.04159 m/s, respectively. Figure 10(b) shows the fluid has two velocities both in the x and y directions after the fluid enters the crevice, and a small part of the fluid will be "squeezed" into the crevice from the y-direction when the fluid enters the crevice. Fluid in the crevice will be "discharged" into the surrounding area after flowing for a certain distance. This phenomenon is because the velocity in the crevice is higher than in other areas. Pressure at the entrance of the crevice is lower than the surrounding area under the action of viscous resistance, so a large velocity gradient will generate after the fluid enters the crevice. At the same time, the viscous resistance in the crevice is extremely low which results in almost no pressure loss in the crevice. The fluid around the crevice is hindered by viscous resistance, so the pressure in the crevice will be higher than the surrounding area after the fluid flows for a certain distance, then the fluid will be "exhausted" from the crevice to the surrounding area. Figure 11 shows the velocity distribution in the crevice of cases 2 and 3 are similar, and the average velocity for the two cases is 6.43×10^{-3} m/s and 9.9065×10^{-4} m/s, respectively.

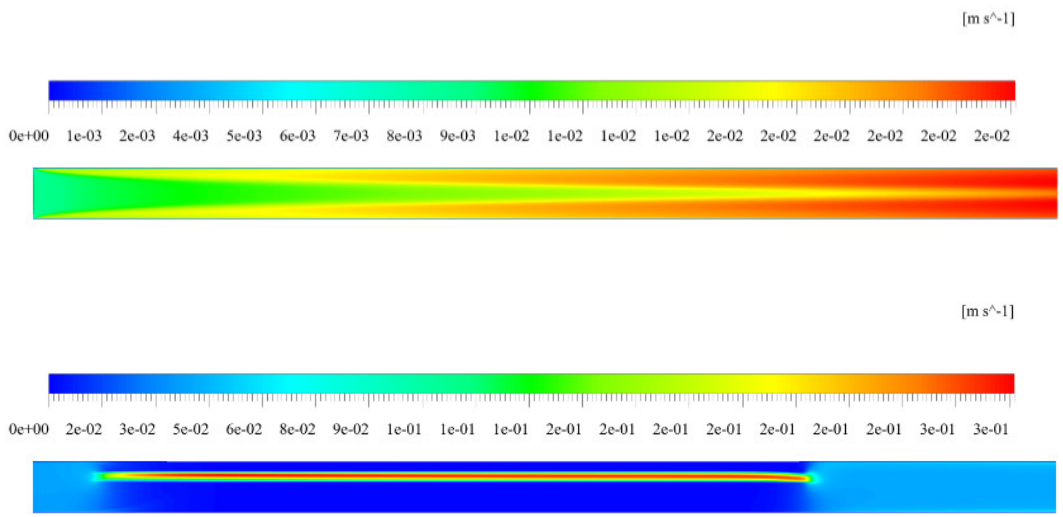

(a) Contours of the velocity distribution without crevice and with a single crevice, respectively

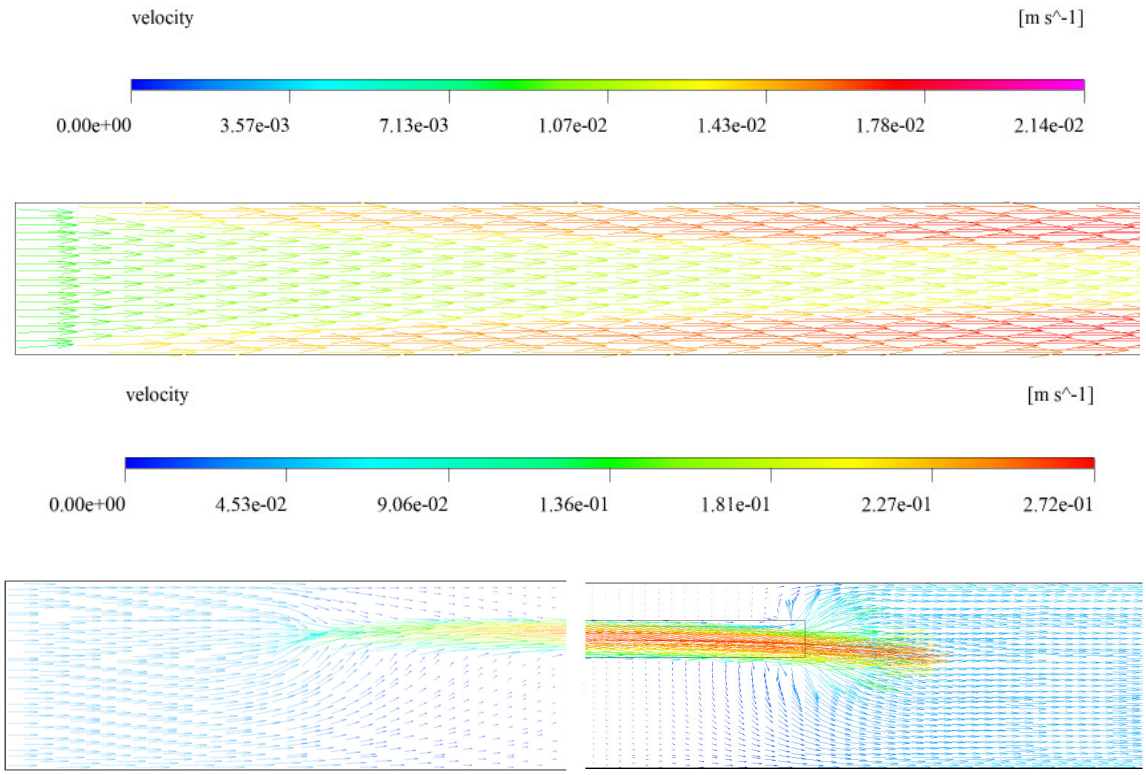

(b) Velocity vector without crevice and with a single crevice, respectively, and the left diagram is the entrance of crevice the right diagram is the export of crevice

Figure 10. Velocity contours and part of vector (case 1) without crevice and with single crevice, respectively.

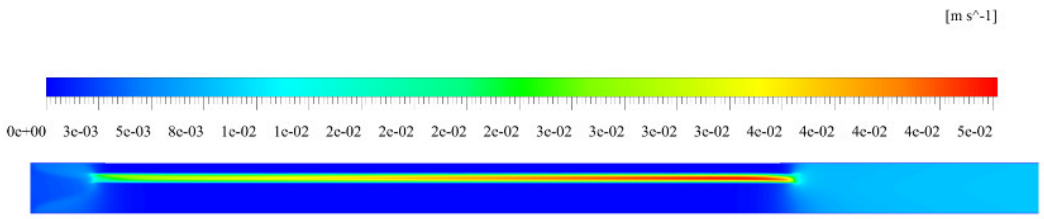

(a) case 2 (γ=0.15, α =4.878×10^{-11})

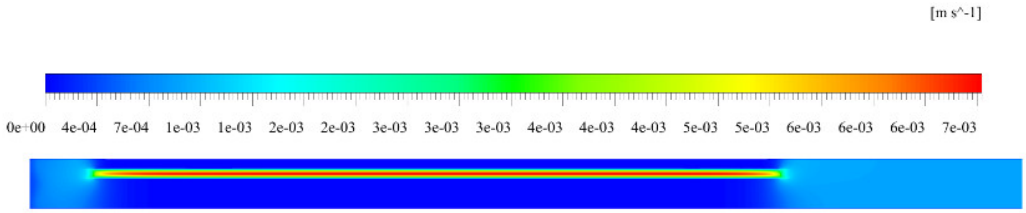

(b) case 3 (γ=0.10, α =6.636×10^{-12})

Figure 11. Velocity contours with a single crevice.

Figure 12 is the temperature distribution contours diagram in cases without crevice and with a single crevice, respectively. Figure 12 shows the existence of a crevice has a great influence on the temperature distribution. Firstly, the temperature distribution feature in the case of the single crevice is low in the crevice and high around the crevice because the velocity is extremely slow around the crevice, so the fluid has sufficient heat exchange time. The temperature in the crevice is lower than the surrounding area, and most of the fluid flows along the crevice if the crevice exists. On the other hand, there is a larger temperature gradient when fluid flows out of the crevice, because the hot and cold parts of the hydrothermal fluid mix when the hydrothermal fluid flows out of the crevice. Secondly, the existence of the crevice makes the average temperature decrease in the entire flow field. It can be seen from Figure 13 that the average temperature with the 0.2 porosity case is reduced by 7.264 °C, the average temperature with the 0.15 porosity case is reduced by 20.955 °C, and the average temperature with the 0.1 porosity case is reduced by 0.122 °C. This phenomenon is caused by the decreased heat flux from the wall, because the crevice causes the near-wall temperature to rise higher after the hydrothermal fluid flows over the same distance. The difference between the near-wall and wall temperatures decreases, leading to the total heat flux decreasing. Thirdly, the degree of total heat flux reduction is different in these cases. Figure 12 shows there is a magnitude difference between the temperature in the crevice and the wall temperature when the porosity is 0.2, and the temperature in the crevice is already close to the wall temperature when the porosity is 0.15 and 0.1. The difference between the temperature in the crevice and the wall temperature leads to the degree of average temperature reduction is different.

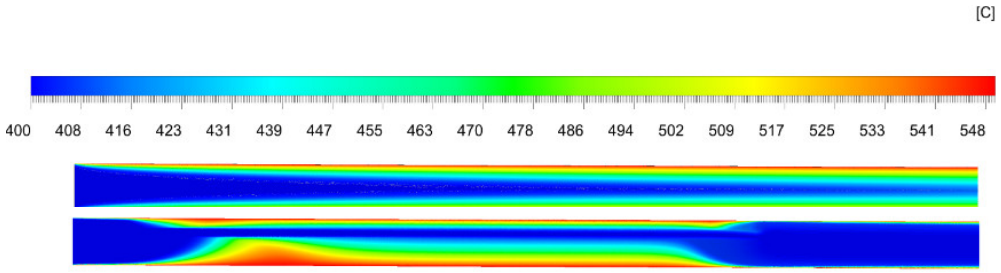

(a) case 1 (γ=0.2, α=3.737×10^{-10} m^2)

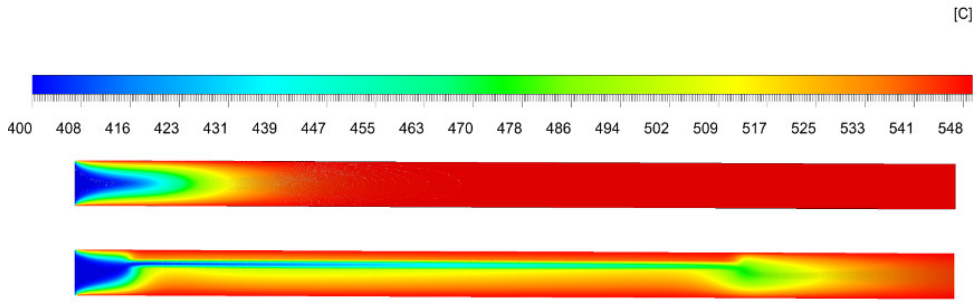

(b) case 2 (γ=0.15, α=4.878×10^{-11})

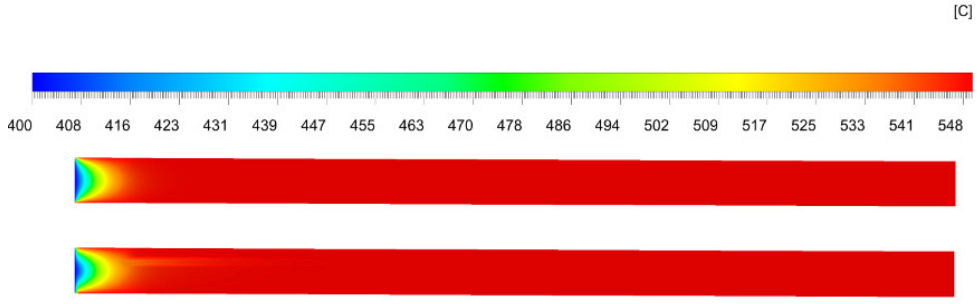

(c) case 3 (γ=0.10, α=6.636×10^{-12})

Figure 12. Temperature contours without crevice and with a single crevice, respectively.

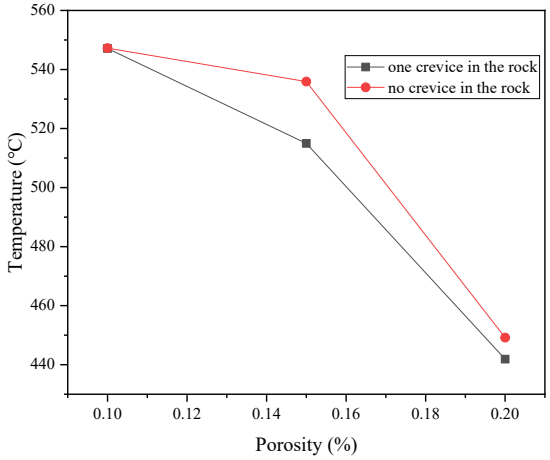

Figure 13. The average temperature under different porosity without crevice and with a single crevice, respectively.

4. Conclusions

The following conclusions can be drawn:

1) The average flow velocity decreases and the average temperature increases when the porosity decreases.

2) Three main parameters affect the trend of the dimensionless velocity in different ranges: the average temperature of the cross-section, the viscous resistance, and the fluid temperature at the center position.

3) The velocity field and temperature field are coupled due to the nonlinear thermophysical properties of hydrothermal. The velocity field and temperature field have strongly interacted in the range of 400–450 ℃ and the effect of temperature on velocity is gradually diminishing outside the range.

4) Most of the fluid will be "squeezed" into the crevice and the average velocity is almost three times the no-creviced case when a crevice is present. The existence of a crevice makes the total heat flux decrease from an overall perspective and makes a large temperature gradient when fluid flows in and out of the crevice from a local perspective.

Acknowledgments

This research was supported by "the Fundamental Research Funds for the Central Universities", 3072020CFT303.

Conflict of interest

The authors declare there is no conflict of interest.

References

1. J. W. Elder, Physical processes in geothermal areas, *Terr. Heat Flow*, **8** (1965), 211–239. https://doi.org/10.1029/GM008p0211
2. J. B. Corliss, J. Dymond, L. I. Gordon, J. M. Edmond, R. P. Herzen, R. D. Ballard, et al., Submarine thermal springs on the galapagos rift, *Science*, **203** (1979), 1073–1083. https://doi.org/10.1126/science.203.4385.1073
3. A. Schultz, J. R. Delaney, R. E. McDuff, On the partitioning of heat flux between diffuse and point source seafloor venting, *J. Geophys. Res.: Solid Earth*, **97** (1992), 12299–12314. https://doi.org/10.1029/92JB00889
4. C. A. Stein, S. Stein, Constraints on hydrothermal heat flux through the oceanic lithosphere from global heat flow, *J. Geophys. Res.: Solid Earth*, **99** (1994), 3081–3095. https://doi.org/10.1029/93JB02222
5. R. P. Lowell, P. A. Rona, R. P. Herzen, Seafloor hydrothermal systems, *J. Geophys. Res.: Solid Earth*, **100** (1995), 327–352. https://doi.org/10.1029/94JB02222
6. P. C. Lichtner, Continuum model for simultaneous chemical reactions and mass transport in hydrothermal systems, *Geochim. Cosmochim. Acta*, **49** (1985), 779–800. https://doi.org/10.1016/0016-7037(85)90172-3

7. E. E. Davis, D. S. Chapman, M. J. Mottl, W. J. Bentkows, K. Dadey, C. Forster, et al., FlankFlux: an experiment to study the nature of hydrothermal circulation in young oceanic crust, *Can. J. Earth Sci.*, **29** (1992), 925–952. https://doi.org/10.1139/e92-078
8. J. U. Bessler, L. Smith, E. E. Davis, Hydrologic and thermal conditions at a sediment/basalt interface: Implications for interpretation of field measurements at Middle Valley, *Proc. Ocean Drill. Program: Sci. Results*, **139** (1994), 667–675. https://doi.org/10.2973/odp.proc.sr.139.253.1994
9. W. L. Taylor, D. D. Pollard, A. Aydin, Fluid flow in discrete joint sets: Field observations and numerical simulations, *J. Geophys. Res.: Solid Earth*, **104** (1999), 28983–29006. https://doi.org/10.1029/1999JB900179
10. T. Jupp, A. Schultz, A thermodynamic explanation for black smoker temperatures, *Nature*, **403** (2000), 880–883. https://doi.org/10.1038/35002552
11. E. E. Davis, K. Becker, J. He, Costa Rica Rift revisited: Constraints on shallow and deep hydrothermal circulation in young oceanic crust, *Earth Planet. Sci. Lett.*, **222** (2004), 863–879. https://doi.org/10.1016/j.epsl.2004.03.032
12. F. J. Fontaine, M. Rabinowicz, J. Boulègue, Permeability changes due to mineral diagenesis in fractured crust: implications for hydrothermal circulation at mid-ocean ridges, *Earth Planet. Sci. Lett.*, **184** (2001), 407–425. https://doi.org/10.1016/S0012-821X(00)00332-0
13. T. J. Crone, W. S. D. Wilcock, Modeling the effects of tidal loading on mid-ocean ridge hydrothermal systems, *Geochem., Geophys., Geosyst.*, **6** (2005), 3021–3045. https://doi.org/10.1029/2004GC000905
14. T. E. Jupp, A. Schultz, A poroelastic model for the tidal modulation of seafloor hydrothermal systems, *J. Geophys. Res.: Solid Earth*, **109** (2004), 1–14. https://doi.org/10.1029/2003JB002583
15. W. S. D. Wilcock, Cellular convection models of mid-ocean ridge hydrothermal circulation and the temperatures of black smoker fluids, *J. Geophys. Res.: Solid Earth*, **103** (1998), 2585–2596. https://doi.org/10.1029/97JB03252
16. Y. Jiang, B. Li, G. Wang, S. Li, New advances in experimental study on seepage characteristics of rock fractures, *Chin. J. Rock Mech. Eng.*, **27** (2008), 2377–2386. https://doi.org/10.3321/j.issn:1000-6915.2008.12.001
17. X. Y. Ma, H. X. Rui, Q. Wang, Experimental study of permeability characteristics of multiscale rock, *Rock Soil Mech.*, **35** (2014), 2191–2196+2204. https://doi.org/10.16285/j.rsm.2014.08.008
18. L. Zhang, H. B. Wang, J. Niu, Y. J. He, Research progrogress of convection heat transfer of supercritical pressure fluid in porous media, *Sci. Technol. Eng.*, **20** (2020), 3808–3816. Available from: https://d.wanfangdata.com.cn/periodical/kxjsygc202010002.
19. P. Alt-Epping, L. W. Diamond, Reactive transport and numerical modeling of seafloor hydrothermal systems: a review, *Magma Microbe: Model. Hydrotherm. Processes Ocean Spreading Cent.*, **178** (2008), 167–192. https://doi.org/10.1029/178GM09
20. S. Wang, S. Zhai, Z. H. Yu, K. Guo, X. Zhang, Reflections on model of modern seafloor hydrothermal system, *Earth Sci.*, **43** (2018), 835–850. https://doi.org/10.3799/dqkx.2018.907
21. E. S. Maayah, H. M. Duwairi, B. Maayah, Analytical model of solar energy storage using non—Newtonian Fluid in a saturated porous media in fully developed region: carboxymethyl cellulose (CMC) and graphite model, *AIMS Energy*, **9** (2021), 213–237. https://doi.org/10.3934/energy.2021012

22. S. C. Zhang, A research on permeability calculation method based on reservoir classification in X area, *China Manganese Ind.*, **37** (2019), 52–56. https://doi.org/10.14101/j.cnki.issn.1002-4336.2019.02.013
23. Y. C. Niu, *The Relationship Between Compression and Resilience Characteristics of Sedimentary Rock and Lithology and Pore Structure*, MA thesis, Northwest University in Xi'an, 2017. Available from: https://kns.cnki.net/kcms/detail/detail.aspx?dbcode=CMFD&dbname=CMFD201801&filename=1017271258.nh&uniplatform=NZKPT&v=ziLL9axxqsZhY_0gSnj1nLmFBITsne5dw5VI2kWI8O6t7I6J6qPP9gmM_3iUvtp2.
24. O. C. Alejandro, A. Perez-Soria, I. Cruz-Maya, V. Guarino, M. A. Alvarez-Perez, Macro-, micro-and mesoporous materials for tissue engineering applications, *AIMS Mater. Sci.*, **5** (2018), 1124–1140. https://doi.org/10.3934/matersci.2018.6.1124
25. P. J. Saccocia, K. M. Gillis, Hydrothermal upflow zones in the oceanic crust, *Earth Planet. Sci. Lett.*, **136** (1995), 1–16. https://doi.org/10.1016/0012-821X(95)00155-5